Chemical Aspects of the Candidate Antiferromagnetic Topological Insulator $MnBi_2Te_4$

Supporting Information

Alexander Zeugner[1], Frederik Nietschke[2], Anja U. B. Wolter[3], Sebastian Gaß[3], Raphael C. Vidal[4], Thiago R. F. Peixoto[4], Darius Pohl[3,5], Christine Damm[3], Axel Lubk[3], Richard Hentrich[3], Simon K. Moser[4,6], Celso Fornari[4], Chul Hee Min,[4] Sonja Schatz[4], Katharina Kißner[4], Maximilian Ünzelmann[4], Martin Kaiser[1], Francesco Scaravaggi[3], Bernd Rellinghaus[3,5], Kornelius Nielsch[3,7,8], Christian Heß[3], Bernd Büchner[3,9], Friedrich Reinert[4], Hendrik Bentmann[4], Oliver Oeckler[2], Thomas Doert[1], Michael Ruck[1,10], Anna Isaeva[3,9*]

1 Faculty of Chemistry and Food Chemistry, Technische Universität Dresden, 01062 Dresden, Germany

2 Institute for Mineralogy, Crystallography and Materials Science, Leipzig University, 04275 Leipzig, Germany

3 Leibniz-Institute for Solid State and Materials Research, 01069 Dresden, Germany

4 Experimentelle Physik VII, Universität Würzburg, 97074 Würzburg, Germany

5 Dresden Center for Nanoanalysis, cfaed, Technische Universität Dresden, 01062 Dresden, Germany

6 Advanced Light Source, Lawrence Berkeley National Laboratory, Berkeley, CA 94720, USA

7 Institute of Materials Science, Technische Universität Dresden, 01062 Dresden, Germany

8 Institute of Applied Physics, Technische Universität Dresden, 01062 Dresden, Germany

9 Institute of Solid State Physics, Technische Universität Dresden, 01062 Dresden, Germany

10 Max Planck Institute for Chemical Physics of Solids, 01187 Dresden, Germany

1. Powder Synthesis of $MnBi_2Te_4$

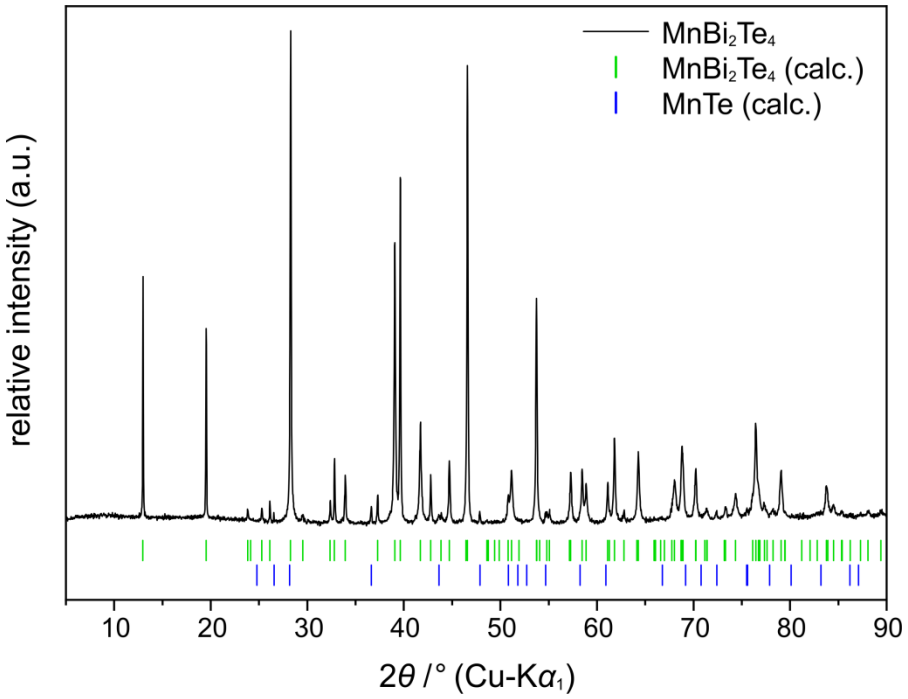

Figure S1. PXRD of a powder sample with the initial composition $MnBi_2Te_4$ (sample #1). The sample was synthesized from the elements following the procedure in Ref. [25]. Note the texture of (00*l*) reflections in contrast to Figure 1 in the main text (sample #2).

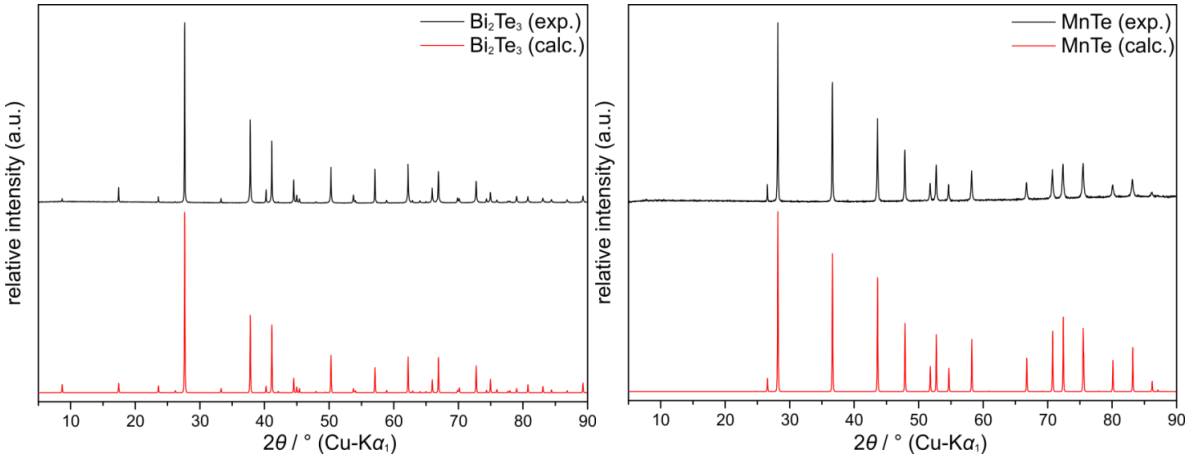

Figure S2. Theoretical (red) and experimental (black) PXRD patterns of the binary Bi_2Te_3 and α-MnTe precursors used in the solid-state synthesis of $MnBi_2Te_4$.

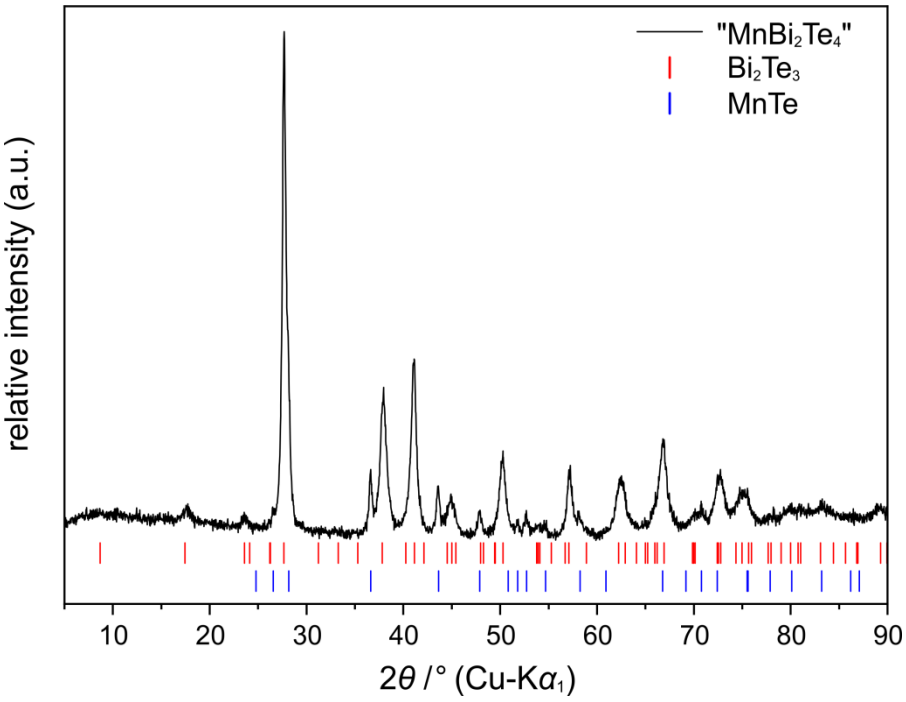

Figure S3. Experimental PXRD pattern of a mixture of Bi_2Te_3 and MnTe (molar ratio 1:1) after mechanical activation by ball milling.

2. Thermal Stability of $MnBi_2Te_4$

Thermal behavior of $MnBi_2Te_4$ was comprehensively studied by differential scanning calorimetry (DSC).

1) At first, a stoichiometric mixture of the binary precursors was mechanically activated (Figure S3) and subjected to two consecutive heating-and-cooling cycles from room temperature to 800 °C (Figure S4). The tentative assignment of the observed signals is listed in Table S1. Comparison of the DSC data and the PXRD pattern after the DSC (Figure S5) indicate that an additional ternary phase (labeled **X** hereafter) with a lower Mn-content exists in the Mn–Bi–Te system. According to our preliminary EDX data, it contains approx. 7–8 at. % Mn. In close analogy with the $(GeTe)(Bi_2Te_3)_n$ homologous series, it could contain both (Bi_2Te_3) and ($MnBi_2Te_4$) slabs. The details will be reported elsewhere. Bi_2Te_3 melts congruently at about 586 °C, while α-MnTe undergoes several phase transitions before melting incongruently at temperatures above 1100 °C[1]. The first two endothermic signals in the first heating curve (Figure S4) are attributed to the melting of Bi_2Te_3 (#1) and the directly following melting of phase **X**. Partial melting of the mixture seems to increase mobility and solubility of solid α-MnTe in the liquid phase, so that the formation of $MnBi_2Te_4$ (exothermic signal #3) and its subsequent melting (signal #4) proceed just about 11 °C higher. The corresponding first cooling run shows two exothermic crystallization signals that we assign to the crystallization of $MnBi_2Te_4$ (signal #1) and almost simultaneous solidification of the phase **X** and Bi_2Te_3 (overlapping signals #2). The second run mostly replicates the first one with the only omission of the exothermic reaction signal upon heating. The phase analysis of the ingot after the DSC experiment yields a mixture of the starting materials (Bi_2Te_3 and α-MnTe) with a significant portion of $MnBi_2Te_4$ and admixtures of phase **X** (Figure S5). Additional EDX investigations corroborate the presence of ternary compounds with strong variations of the Mn content (between 2 and 14 at. %).

[1] Binary Alloy Phase Diagrams. 2nd Edition. Ed. T. B. Massalski, ASM International, Materials Park, Ohio, 1990.

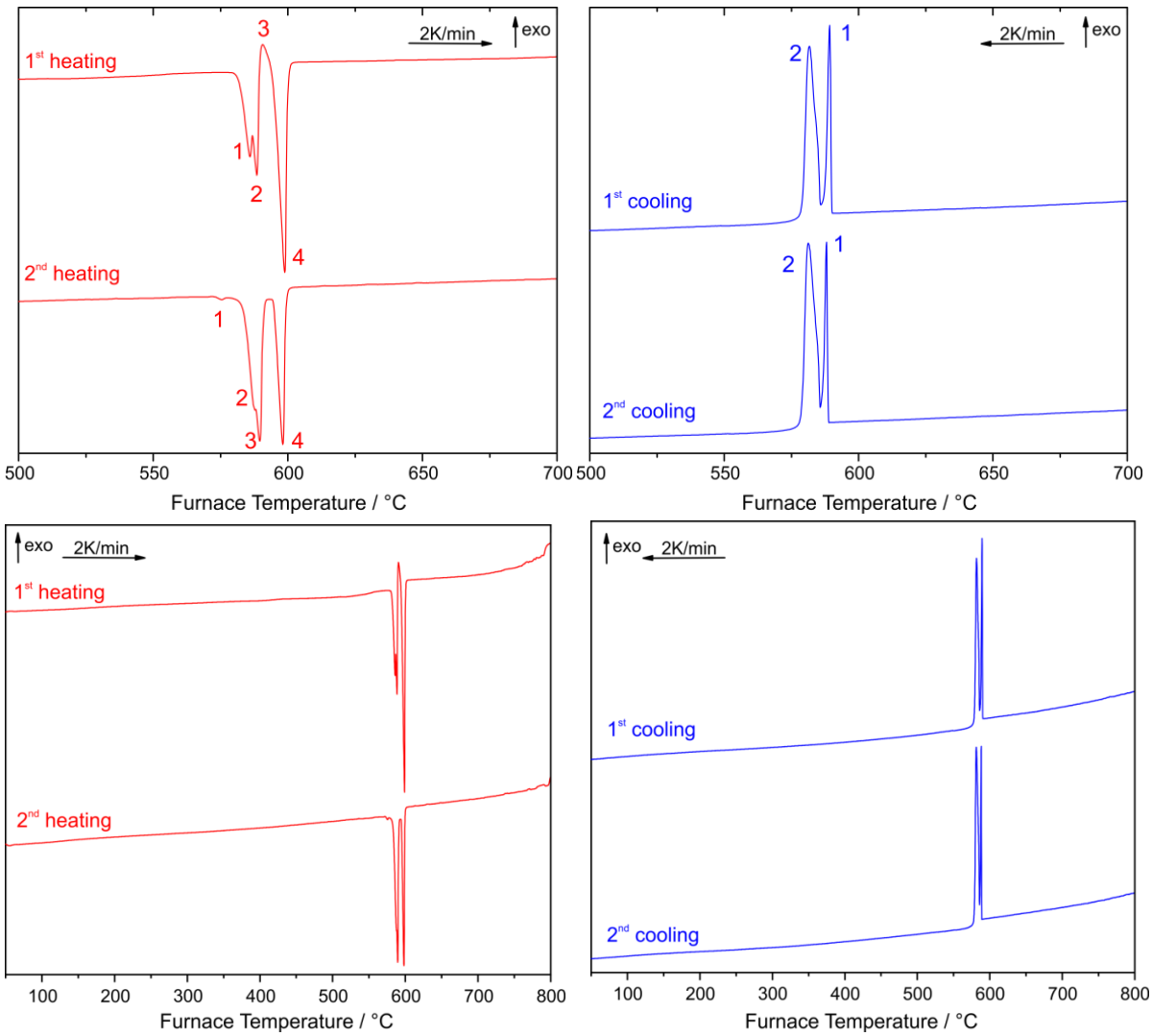

Figure S4. Heating (red) and cooling (blue) runs of the DSC experiment on a mechanically activated stoichiometric mixture of Bi_2Te_3 and MnTe. The bottom row shows unabridged curves recorded from room temperature up to 800 °C.

Table S1. Attribution of the signals in Figure S4.

Run	Signal	T_{peak} / °C	Tentative assignment
1st heating	1	586.0	Melting of Bi_2Te_3
	2	588.5	Melting of ternary phase **X**
	3	590.7	Formation of $MnBi_2Te_4$
	4	598.9	Melting of $MnBi_2Te_4$
1st cooling	1	589.3	Solidification of $MnBi_2Te_4$
	2	581.6	Co-solidification of ternary phase **X** and Bi_2Te_3
2nd heating	1	575.4	Melting of Bi-richer Bi_xTe_y (a shift in temperature compared to Bi_2Te_3)
	2	587.8	Melting of Bi_2Te_3
	3	589.6	Melting of phase **X**
	4	598.1	Melting of $MnBi_2Te_4$
2nd cooling	1	588.1	Solidification of $MnBi_2Te_4$
	2	581.3	Co-solidification of ternary phase **X** and Bi_2Te_3

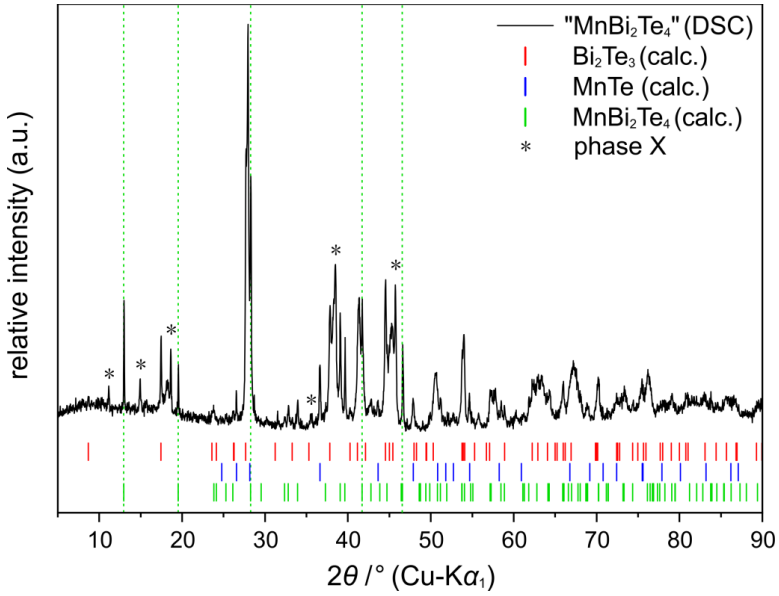

Figure S5. PXRD of the sample with the initial composition $MnBi_2Te_4$ after the DSC experiment presented in Figure S4.

2) Another DSC experiment was performed on the presynthesized powder of $MnBi_2Te_4$ (sample #1) that contained approx. 4 wt. % of MnTe (Figure S1). Its thermal stability was first examined (heating and cooling cycles at 2 K/min) from room temperature up to 400 °C. No thermal signals were observed in the DSC curves (not shown here). Only minor changes in the PXRD (Figure S6) were found after the experiment, i. e. additionally approx. 5 wt. % of Bi_2Te_3 from a Rietveld refinement. In other words, after two consecutive heating–cooling cycles up to 400 °C sample #1 was still dominated by $MnBi_2Te_4$. The same sample subjected to temperature-programmed powder diffraction (see main text) started to decompose already at 200 °C, probably due to the smaller grain size (see below). Another fraction of the same sample was examined by DSC above the melting point of Bi_2Te_3 and showed the melting signals of Bi_2Te_3 and $MnBi_2Te_4$ (Figure S7). The signals in the cooling curves were identical to those in Figure 1 of the main text and Figure S4. After crystallization in the DSC experiment this sample contained $MnBi_2Te_4$, Bi_2Te_3, MnTe and phase **X** (Figure S8). In contrast to Ref. [**Error! Bookmark not defined.**], we have not observed any signs of $MnTe_2$ (Figure S8).

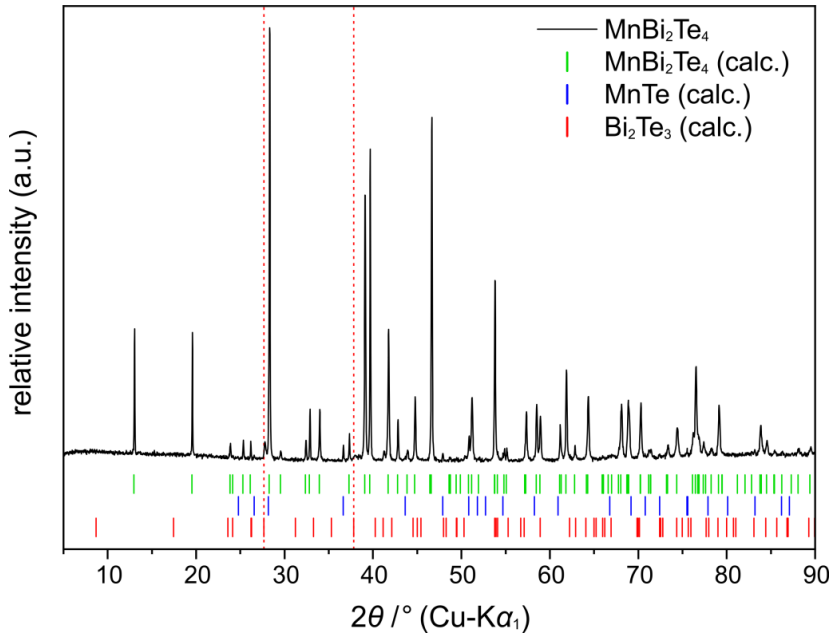

Figure S6. PXRD of the sample #1 (initial composition $MnBi_2Te_4$) after two consecutive DSC heating and cooling cycles from room temperature to 400 °C.

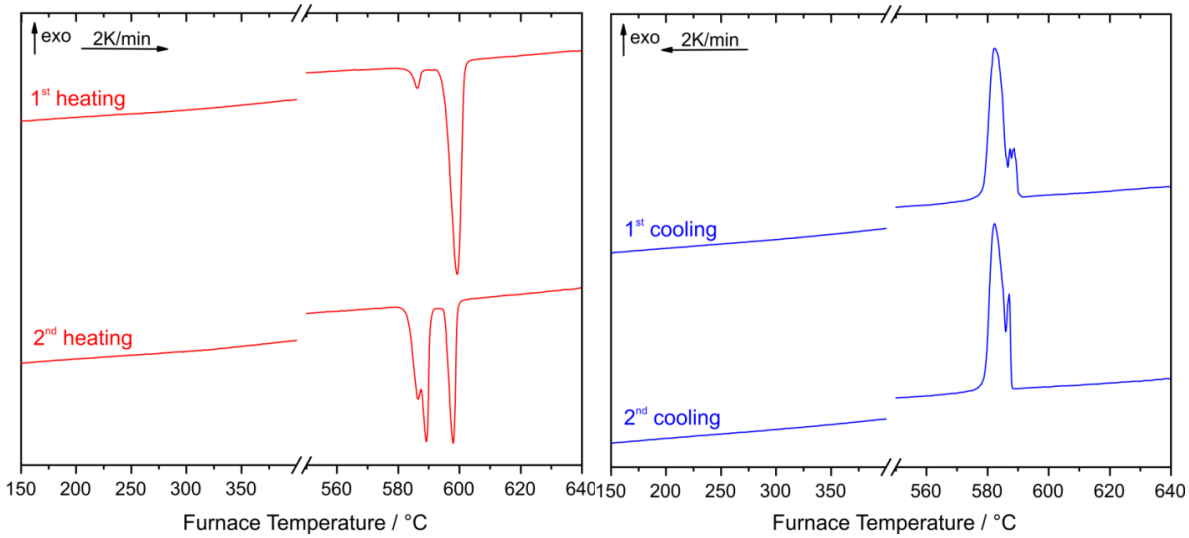

Figure S7. Excerpts from the DSC experiment on sample #1: cut-outs showing the region of the expected decomposition (150–400 °C) and the region of the melting/solidification at around 590 °C. The first heating DSC curve shows a signal of Bi_2Te_3 melting in contrast to the sample #2 prepared via a solid-state route from the binaries.

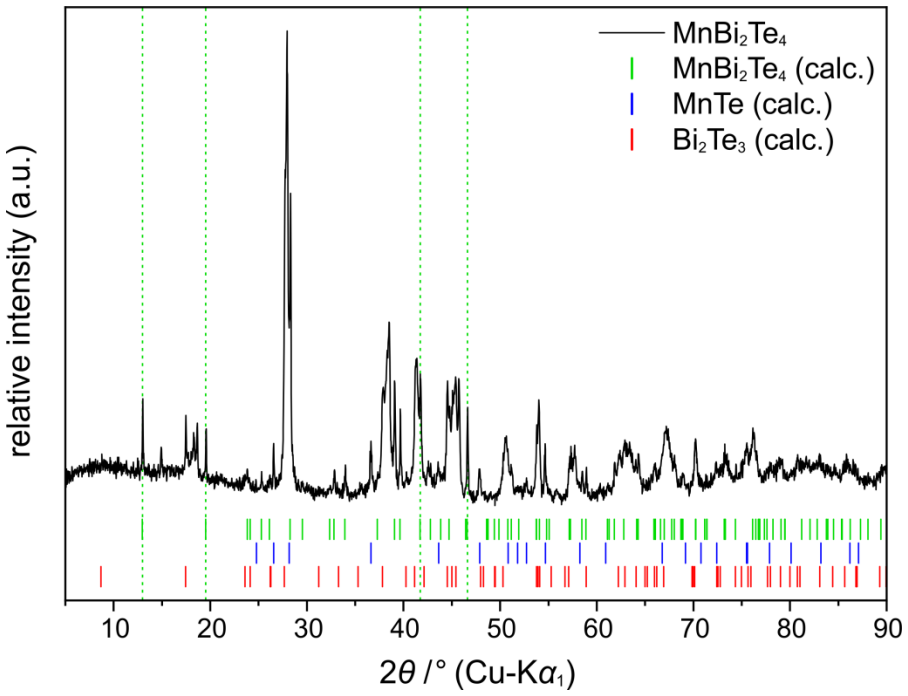

Figure S8. PXRD of the sample #1 (initial composition $MnBi_2Te_4$) after two consecutive DSC heating and cooling cycles from room temperature to 800 °C.

3) The results of the DSC experiments on sample **#2** are qualitatively the same as described above in 2). The exact nature of a signal overlapping with the melting signal of $MnBi_2Te_4$ in the first heating curve (Fig. 1 in the main text) is not clear. The second heating and cooling cycle was identical to that given in Figure S7 and is therefore discussed above.

$MnBi_2Te_4$ (sample #2) was found to decompose gradually into Bi_2Te_3 and MnTe during annealing at 400 °C (Figure 1). The amount of binaries steadily increased with the experiment's duration, but the full decomposition has not been observed after 5 days. Annealing of bulk sample #1 at 200 °C also very slowly leads to decomposition into Bi_2Te_3 and manganese tellurides during several days. Remarkably, this decomposition seems irreversible unless the mixture is fused again; $MnBi_2Te_4$ is regained after the repeated procedure applied during synthesis of sample #1. This may be due to macroscopic phase separation during the annealing process. Note that decomposition is much faster during HT-PXRD, probably as a powder with much smaller grain size was used. Thus, decomposition may be delayed in compact bulk material, e. g. due to the influence of strain on diffusion and phase formation.

The phase composition and crystallinity of larger bulk samples depend on the quenching/cooling rates. Stoichiometric mixtures (molar ratio 1:1) of ball-milled binary precursors Bi_2Te_3 and MnTe were fused at 650 °C and slowly cooled at various rates. Quenching of the melt results in a poorly ordered Bi2Te3-like phase accompanied by small amounts of α-MnTe and, presumably, unknown ternary compounds (Figure S9). At sufficiently slow cooling rates (6 K/h), the fraction of $MnBi_2Te_4$ significantly increases (Figure S10).

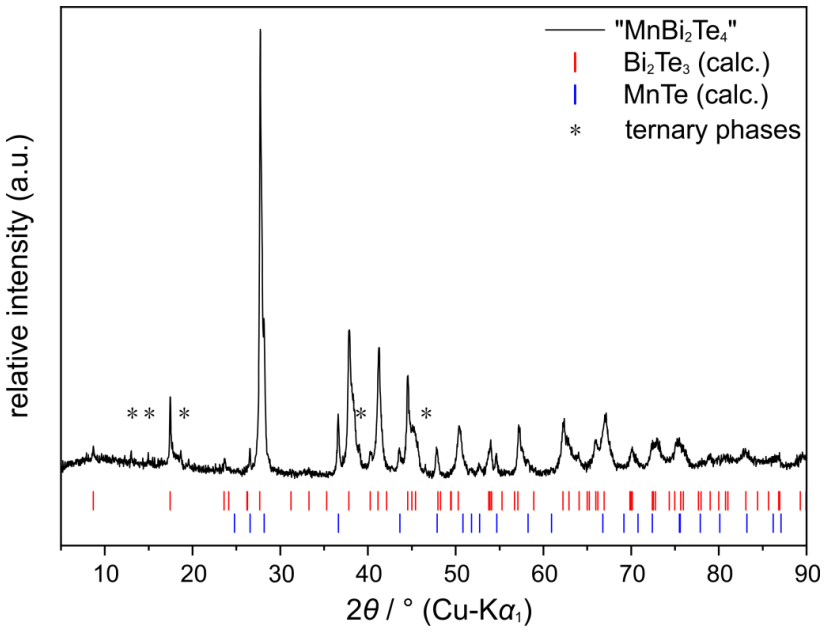

Figure S9. PXRD of the sample with the initial composition $MnBi_2Te_4$ that was fused at 650 °C and quenched.

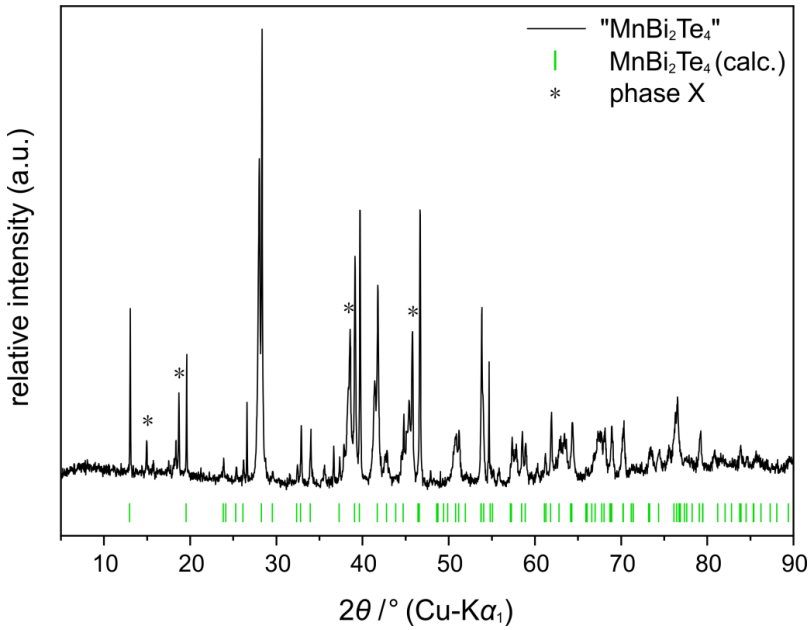

Figure S10. PXRD of the sample with the initial composition $MnBi_2Te_4$ that was fused at 650 °C and cooled down to room temperature at the rate of 6 K/h. See above about the phase **X**.

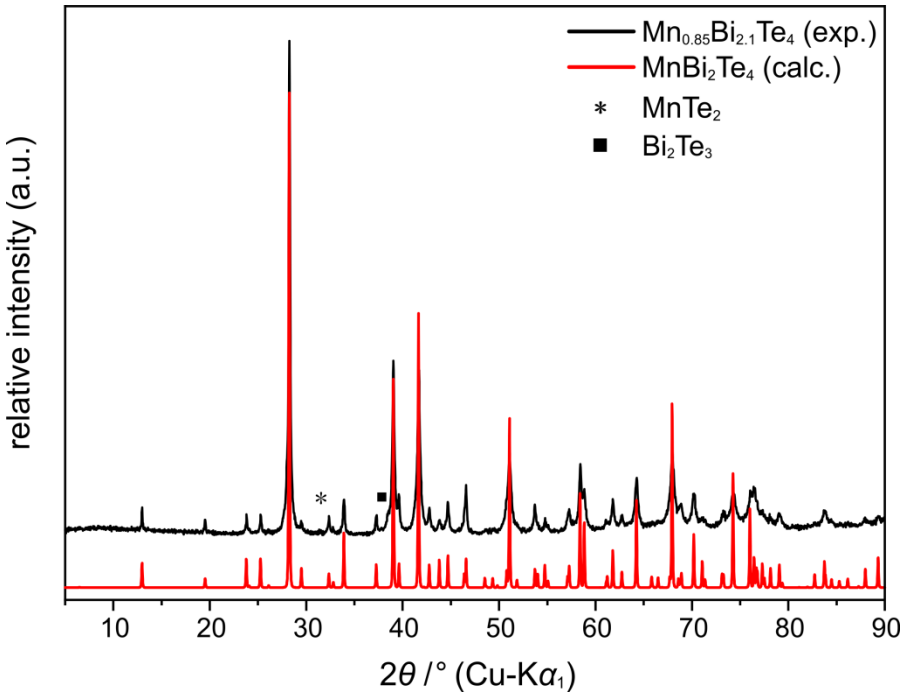

Figure S11. Calculated (red) and experimental (black) PXRD patterns of $Mn_{0.85}Bi_{2.1}Te_4$. This sample was prepared by the route #2 from a mixture of binaries by a solid-state reaction at 565 °C. The strongest reflections of $MnTe_2$ and Bi_2Te_3 admixtures are marked by an asterisk and a filled square. Note that the PXRD pattern of a sample with the same composition but synthesized via route **#1** was similar.

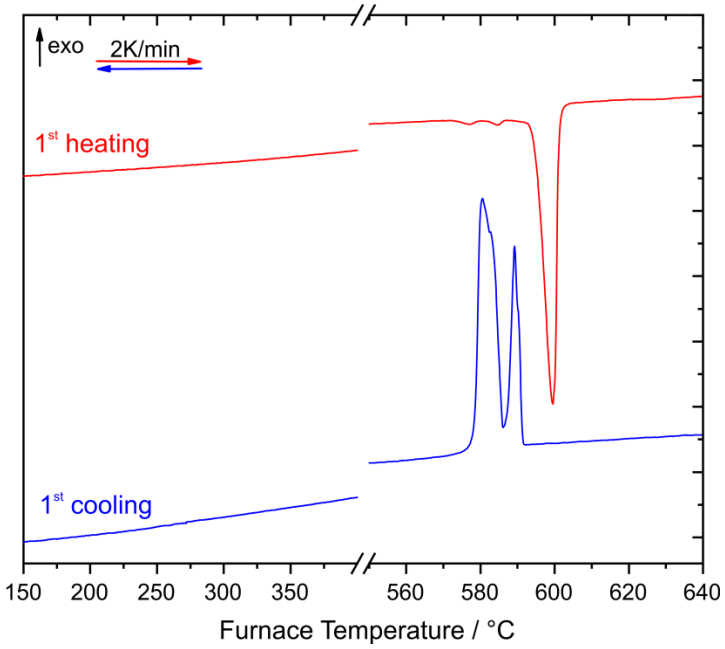

Figure S12. Excerpts from the DSC experiment on $Mn_{0.85}Bi_{2.1}Te_4$: cut-outs showing the region of the expected decomposition (150–400 °C) and the region of the melting/solidification at around 590 °C. The second heating and cooling cycle was similar to that in Figure S7 and is therefore discussed above.

3. Crystal Structure Elucidation of the Non-Stoichiometric $Mn_{0.85(3)}Bi_{2.10(3)}Te_4$ Model

Table S2. Coefficients U_{ij} (in pm^2) of the tensors of the anisotropic displacement, and equivalent isotropic displacement parameters for the atoms in $Mn_{0.85(3)}Bi_{2.10(3)}Te_4$. U_{eq} is defined as one third of the trace of the orthogonalized U_{ij} tensor. For all atoms $U_{23} = U_{13} = 0$.

Atom	U_{11}	U_{22}	U_{33}	U_{12}	U_{eq}
Bi1	166(1)	166(1)	213(1)	83(1)	182(1)
Bi2	169(2)	169(2)	179(3)	85(1)	172(1)
Mn1	166(1)	166(1)	213(1)	83(1)	182(1)
Mn2	169(2)	169(2)	179(3)	85(1)	172(1)
Te1	177(1)	177(1)	155(1)	88(1)	170(1)
Te2	161(1)	161(1)	185(1)	80(1)	169(1)

Table S3. Selected interatomic distances (/pm) and bond angles (/°) for $Mn_{0.85(3)}Bi_{2.10(3)}Te_4$.

Bi1/Mn1—Te1	329.1(1)	Te2—Bi1/Mn1—Te2	91.4(1)
Bi1/Mn1—Te2	302.7(1)	Te2—Bi1/Mn1—Te1	93.0(1)
Bi2/Mn2—Te1	297.7(1)	Te1—Bi2/Mn2—Te1	93.3(1)
Te2···Te2	369.9(1)	Bi2/Mn2—Te1—Bi1/Mn1	91.9(1)

4. Crystal Structure Elucidation of the Stoichiometric $MnBi_2Te_4$ Model

Table S4. Crystallographic data for $MnBi_2Te_4$, refined with antisite defects in both cation positions, from SCXRD data.

Crystal system, space group	**trigonal, $R\bar{3}m$ (no. 166)**
Formula units	$Z = 3$
Lattice parameters	$a = 433.14(2)$ pm $c = 4093.2(2)$ pm $V = 665.1(1) \times 10^6$ pm^3 $\rho_{calc.} = 7.37$ g cm^{-3}
Temperature	250(2) K
Range for data collection; index ranges	$2.98° \leq 2\theta \leq 93.81°$ ($\lambda = 71.073$ pm); $-8 \leq h \leq 8$, $-8 \leq k \leq 8$, $-84 \leq l \leq 83$;
Collected reflections	10795 measured, 852 unique
***R* indices of merging**	$R_{int} = 0.079$, $R_\sigma = 0.044$
Structure refinement	Full-matrix least-squares based on F^2, anisotropic displacement parameters
Data/restraints/parameters	852/1/14
Final R indices and goodness-of-fit on F^2	$R1[602\, F_o > 4\sigma(F_o)] = 0.024$ $wR2$ (all F_o^2) = 0.035 $GooF = 1.053$
Min./max. residual electron density	$-4.06/2.84$ e $\times 10^{-6}$ pm^{-3}

Table S5. Synopsis of the coordinates, equivalent displacement parameters, and occupancies for the stoichiometric $MnBi_2Te_4$ model, with antisite defects in both cation positions.

Bi_2MnTe_4, SCXRD					
atom	x	y	z	U_{eq}/pm^2	occ.
Bi1 6*c*	1/3	2/3	0.09173(2)	178(1)	0.912(1)
Bi2 3*a*	0	0	0	160(2)	0.175(1)
Mn1 6*c*	1/3	2/3	0.09173(2)	178(1)	0.088(1)
Mn2 3*a*	0	0	0	160(2)	0.825(1)
Te1 6*c*	2/3	1/3	0.03947(2)	176(1)	1
Te2 6*c*	0	0	0.133338(2)	176(1)	1

Table S6. Coefficients U_{ij} (in pm^2) of the tensors of the anisotropic displacement, and equivalent or isotropic displacement parameters for the atoms in the stoichiometric $MnBi_2Te_4$ model. U_{eq} is defined as one third of the trace of the orthogonalized U_{ij} tensor. For all atoms $U_{23} = U_{13} = 0$.

Atom	U_{11}	U_{22}	U_{33}	U_{12}	U_{eq}
Bi1	162(1)	162(1)	211(1)	81(1)	178(1)
Bi2	156(2)	156(2)	167(3)	78(1)	160(2)
Mn1	162(1)	162(1)	211(1)	81(1)	178(1)
Mn2	156(2)	156(2)	167(3)	78(1)	160(2)
Te1	184(1)	184(1)	162(1)	92(1)	176(1)
Te2	168(1)	168(1)	192(2)	84(1)	176(1)

Table S7. Selected interatomic distances (/pm) and bond angles (/°) for $MnBi_2Te_4$.

Bi1/Mn1—Te1	329.1(1)	Te2—Bi1/Mn1—Te2	91.4(1)
Bi1/Mn1—Te2	302.6(1)	Te2—Bi1/Mn1—Te1	93.0(1)
Bi2/Mn2—Te1	297.7(1)	Te1—Bi2/Mn2—Te1	93.3(1)
Te2···Te2	369.9(1)	Bi2/Mn2—Te1—Bi1/Mn1	91.9(1)

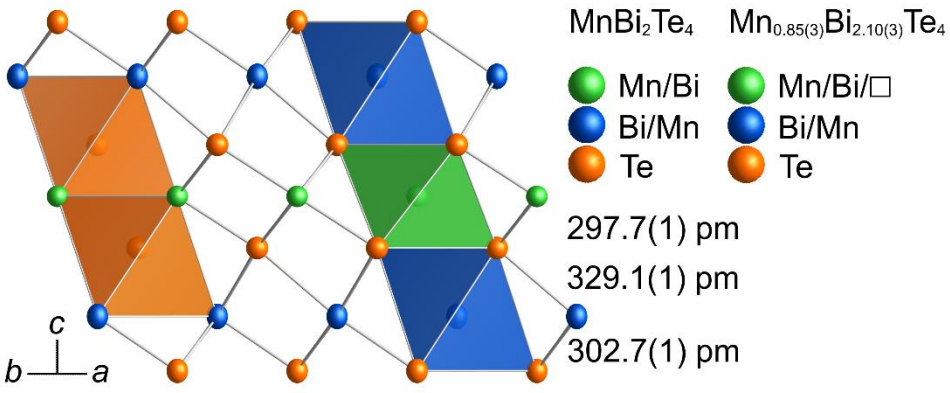

Figure S13. A single septuple layer of $Mn_{1-x}Bi_{2+2x/3}Te_4$ showing schematically the two considered structure refinements. Mn–Te1, Bi–Te1 and Bi–Te2 bond lengths indicated. Ellipsoids enclose 90 % of the probability density.

5. **Thermoelectric Characterization of $Mn_{0.85}Bi_{2.1}Te_4$**

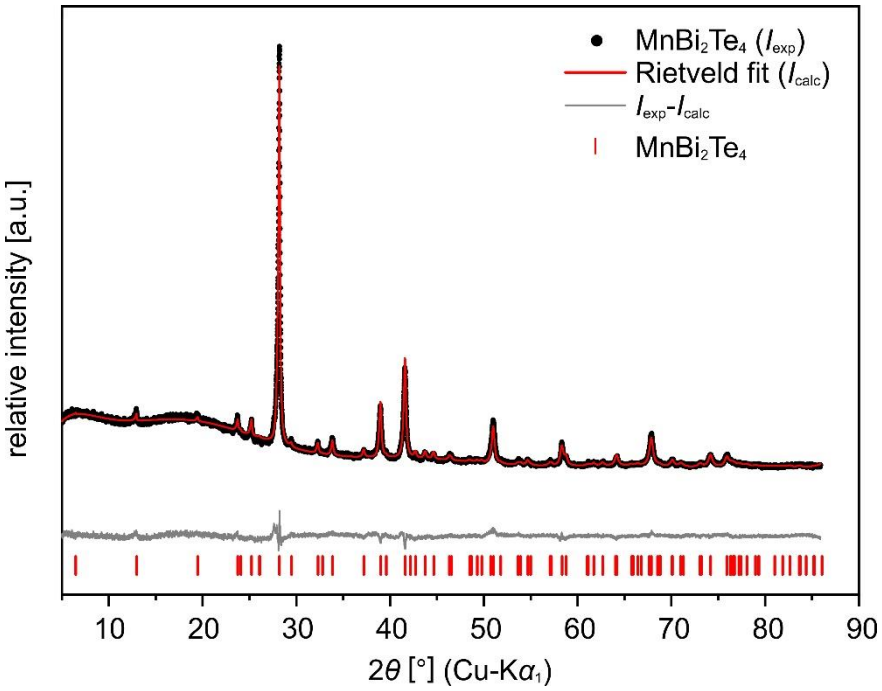

Figure S14. Rietveld refinement for a $Mn_{0.85}Bi_{2.1}Te_4$ sample (synthesized by route **#1**) before the thermoelectric characterization. R_{WP} = 0.018, refined lattice parameters: a = 4.3226 Å, c = 40.798 Å.

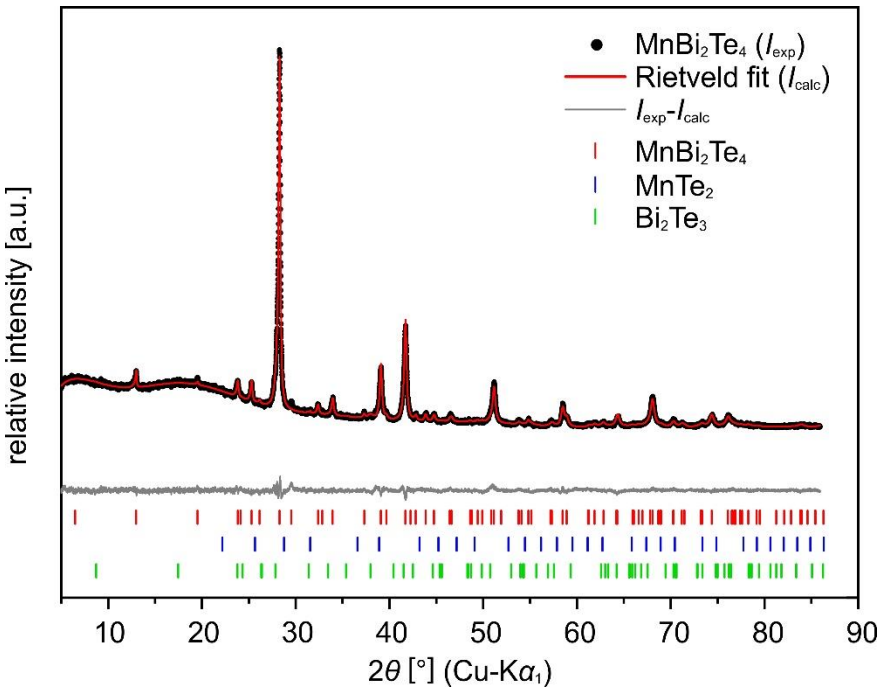

Figure S15. Rietveld refinement for a $Mn_{0.85}Bi_{2.1}Te_4$ sample after the thermoelectric characterization, showing minor decomposition: $Mn_{0.85}Bi_{2.1}Te_4$ (86 wt. %), Bi_2Te_3 (13 wt.%) und $MnTe_2$ (< 1 wt.%). R_{WP} = 0.021.